

Spin transfer nano-oscillator based on synthetic antiferromagnetic skyrmion pair assisted by perpendicular fixed magnetic field

Yun-Xu Ma(马云旭), Jia-Ning Wang(王佳宁), Zhao-Zhuo Zeng(曾钊卓), Ying-Yue Yuan(袁映月), Jin-Xia Yang(杨金霞), Hui-Bo Liu(刘慧博), Sen-Fu Zhang(张森富), Jian-Bo Wang(王建波), Chen-Dong Jin(金晨东), and Qing-Fang Liu(刘青芳)

Citation: Chin. Phys. B, 2022, 31 (**10**): 100501. DOI: 10.1088/1674-1056/ac6ee4
Journal homepage: http://cpb.iphy.ac.cn; http://iopscience.iop.org/cpb

What follows is a list of articles you may be interested in

Finite-time synchronization of uncertain fractional-order multi-weighted complex networks with external disturbances via adaptive quantized control

Hongwei Zhang(张红伟), Ran Cheng(程然), and Dawei Ding(丁大为)†
Chin. Phys. B, 2022, 31 (**10**): 100504. DOI: 10.1088/1674-1056/ac686b

Improved functional-weight approach to oscillatory patterns in excitable networks

Tao Li(李涛), Lin Yan(严霖), and Zhigang Zheng(郑志刚)
Chin. Phys. B, 2022, 31 (**9**): 090502. DOI: 10.1088/1674-1056/ac7458

Power-law statistics of synchronous transition in inhibitory neuronal networks

Lei Tao(陶蕾) and Sheng-Jun Wang(王圣军)
Chin. Phys. B, 2022, 31 (**8**): 080505. DOI: 10.1088/1674-1056/ac5c31

Explosive synchronization: From synthetic to real-world networks

Atiyeh Bayani, Sajad Jafari, and Hamed Azarnoush
Chin. Phys. B, 2022, 31 (**2**): 020504. DOI: 10.1088/1674-1056/ac3cb0

Robust H_∞ state estimation for a class of complex networks with dynamic event-triggered scheme against hybrid attacks

Yahan Deng(邓雅瀚), Zhongkai Mo(莫中凯), and Hongqian Lu(陆宏谦)
Chin. Phys. B, 2022, 31 (**2**): 020503. DOI: 10.1088/1674-1056/ac0ee9

Spin transfer nano-oscillator based on synthetic antiferromagnetic skyrmion pair assisted by perpendicular fixed magnetic field

Yun-Xu Ma(马云旭)[1], Jia-Ning Wang(王佳宁)[1], Zhao-Zhuo Zeng(曾钊卓)[1], Ying-Yue Yuan(袁映月)[1], Jin-Xia Yang(杨金霞)[1], Hui-Bo Liu(刘慧博)[1], Sen-Fu Zhang(张森富)[1], Jian-Bo Wang(王建波)[1,2], Chen-Dong Jin(金晨东)[3], and Qing-Fang Liu(刘青芳)[1,†]

[1] *Key Laboratory for Magnetism and Magnetic Materials of the Ministry of Education, Lanzhou University, Lanzhou* 730000, *China*
[2] *Key Laboratory for Special Function Materials and Structural Design of the Ministry of Education, Lanzhou University, Lanzhou* 730000, *China*
[3] *College of Physics Science and Technology, Hebei University, Baoding* 071002, *China*

(Received 10 March 2022; revised manuscript received 27 April 2022; accepted manuscript online 12 May 2022)

As a microwave generator, spin transfer nano-oscillator (STNO) based on skyrmion promises to become one of the next-generation spintronic devices. However, there still exist a few limitations to the practical applications. In this paper, we propose a new STNO based on synthetic antiferromagnetic (SAF) skyrmion pair assisted by a perpendicular fixed magnetic field. It is found that the oscillation frequency of this kind of STNO can reach up to 5.0 GHz, and the multiple oscillation peak with higher frequency can be realized under a fixed out-of-plane magnetic field. Further investigation shows that the skyrmion stability is improved by bilayer antiferromagnetic coupling, which guarantees the stability process of skyrmion under higher spin-polarized current density. Our results provide the alternative possibilities for designing new skyrmion-based STNO to further improve the oscillation frequency, and realize the output of multiple frequency microwave signal.

Keywords: nano-oscillator, skyrmion, spin-polarized current, spintronic devices

PACS: 05.45.Xt, 12.39.Dc, 72.25.Hg, 85.75.–d **DOI:** 10.1088/1674-1056/ac6ee4

1. Introduction

Spin transfer nano-oscillator (STNO) is a new kind of promising spintronic device that can be used to generate microwave signals.[1,2] For most of STNOs, the structure is usually designed based on the spin valve or magnetic tunnel junction consisting of fixed layer, spacer, and free layer. In this kind of STNO, the magnetic moment of free layer precesses steadily when the spin-polarized current is applied along out-of-plane, and thus outputing an oscillatory microwave signal due to the giant magnetoresistance effect. After that, it is reported that the magnetic domain wall,[3,4] circular vortex,[5–7] radial vortex,[8] droplet,[9,10] and skyrmion[11–16] have been suggested to be used in STNO device. Especially in recent years, owing to high stability, small size, topological protection, and low driven current density, the skyrmion has attracted significant interest in designing spintronic devices as a potential information carrier.[17] Moreover, different types of skyrmions have been observed both theoretically and experimentally. For example, the typical Bloch skyrmion and Néel skyrmion have been observed in bulk magnetic materials with bulk Dzyaloshinskii–Moriya interaction[18–20] and heterostructures with strong orbital coupling,[21–23] respectively. In addition, the synthetic antiferromagnetic (SAF) skyrmion are suggested to overcome skyrmion Hall effect considering their stability and reliability.[24–26] In experiment, it was demonstrated that the synthetic antiferromagnetic skyrmion bubbles can steadily exist at room temperature,[27] and the SAF skyrmion pair has higher velocity than single ferromagnetic skyrmion.[28] Recent report showed that the STNO based on SAF skyrmion pair can reach up to ten GHz.[29] However, this type of STNO based on SAF skyrmion pair only outputs single oscillation frequency microwave signal.

In this paper, we propose to use a fixed magnetic field to further improve oscillation frequency of STNO based on SAF skyrmion pair, and realize a multiple frequency output. The skyrmion process under a magnetic field and spin-polarized current as well as other parameters is studied in detail. Our results show a possible application in designing STNO and further improving its performance.

2. Methods and simulations details

As shown in Fig. 1(a), the STNO based on SAF skyrmion pair is a nanopillar structure consisting of two fixed layers, two spacer layers, two free layers through antiferromagnetic coupling, and a non-magnetic (NM) layer. In the structure, the two fixed layers will excite the same effect of spin transfer torque by respective free layers, thereby ensuring the skyrmion pair to stay the synchronous circular precession. In this way, the spin transfer nano-oscillator based on skyrmion pair generates a stable microwave signal. The free layers are assumed to be all Co magnetic films, where the interfacial Dzyaloshinskii–Moriya interaction (DMI) is generated by Pt with strong spin-

†Corresponding author. E-mail: liuqf@lzu.edu.cn

© 2022 Chinese Physical Society and IOP Publishing Ltd

orbit coupling,[30–32] and the spacer layer and NM layer can be chosen as MgO and Ru,[33] respectively. The diameter of nanopillar is 100 nm, the thickness of two free layers and NM layer are all 1 nm, and the size of mesh cell is set to be 2 nm×2 nm×1 nm. The upward fixed magnetic field is applied to free bilayer along the perpendicular direction. The size of skyrmion pair is the same at the initial state, but the core of skyrmion on the top layer is set to be downward, while the bottom one is upward. Hence, the size of skyrmion in the top layer and the bottom layer are shrunk and enlarged under the upward fixed magnetic field, respectively. Figure 1(b) shows the circular vortex-like magnetization configuration of fixed layer. The SAF skyrmion pair synchronously performs the periodic circular motion when perpendicular spin polarized current is injected into the nanodisk, which exports a stable oscillation voltage signal.

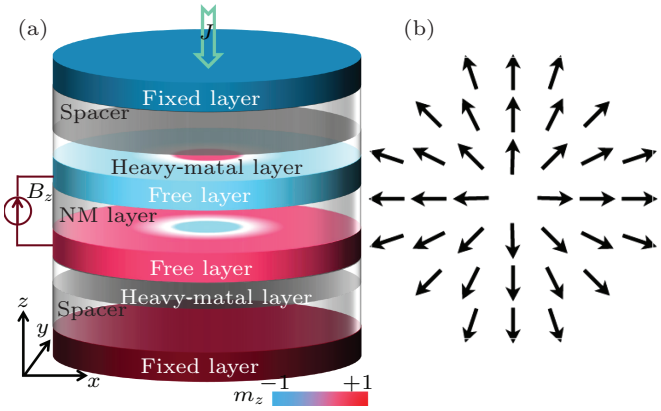


Fig. 1. (a) Schematic diagram of spin transfer nano-oscillator based on synthetic antiferromagnetic skyrmion pair, which is assisted by out-of-plane fixed magnetic field. The total nanopillar structure includes two fixed layers, two spacer layers, two free layers, and one non-magnetic layer. The red and blue colors represent the positive and negative perpendicular magnetization components, respectively. (b) Spin structure of the two fixed layers.

The Object Oriented MicroMagnetic Framework (OOMMF) software is used to investigate the SAF skyrmion pair dynamics,[34] by which the Landau–Lifshitz–Gilbert–Slonczewski (LLGS) equation can be numerically solved for the dynamics of time-dependent magnetization. The equation is given below:[35]

$$\frac{\mathrm{d}\boldsymbol{m}}{\mathrm{d}t} = -\gamma \boldsymbol{m} \times \boldsymbol{H}_{\mathrm{eff}} + \alpha\left(\boldsymbol{m} \times \frac{\mathrm{d}\boldsymbol{m}}{\mathrm{d}t}\right) + \frac{u}{t_{\mathrm{F}}}\boldsymbol{m} \times (\boldsymbol{m}_{\mathrm{p}} \times \boldsymbol{m}), \tag{1}$$

where γ represents the gyromagnetic ratio, and $\boldsymbol{m}$ the unit magnetization vector. The Gilbert damping parameter α is set to be 0.02 for solving the initial state and dynamic process. The u and t_{F} represent the spin-polarized electron velocity and the thickness of the free layer, respectively. The u is described as

$$u = \frac{\gamma \hbar P}{2\mu_0 e M_{\mathrm{s}}} J, \tag{2}$$

where P is the spin polarization which is fixed at 0.4, e is the electron charge, and J is the current density. In addition, $\boldsymbol{m}_{\mathrm{p}}$ denotes the perpendicular magnetization vector. The $\boldsymbol{H}_{\mathrm{eff}}$ is the effective field of the system including the Heisenberg exchange field, the uniaxial perpendicular magnetic anisotropy field, demagnetization field, and Dzyaloshinskii–Moriya effective field. In the simulations, the material parameters of the cobalt film are chosen as follows:[32,36,37] exchange constant $A = 1.5 \times 10^{-11}$ J/m, the uniaxial magnetocrystalline anisotropy constant $K_{\mathrm{u}} = 8 \times 10^5$ J/m^3, saturation magnetization $M_{\mathrm{S}} = 8.6 \times 10^5$ A/m, and the DMI constant $D = 3.0$ mJ/m^2 except for Fig. 4(a). Finally, the interlayer exchange coupling coefficient $\sigma = -1 \times 10^{-4}$ J/m^2 or -1×10^{-3} J/m^2, in which the negative value indicates the bilayer antiferromagnetic coupling. In this case, the SAF skyrmion pair stably exists in the double free layers.

3. Results and discussion

To start with, we study the dynamic process of SAF skyrmion pair under the effect of spin-polarized current assisted by fixed magnetic field as shown in Fig. 2. Figure 2(a) shows the initial state of the SAF skyrmion pair in the free bilayer, *i.e.* the left semicircle for the top layer and right semicircle for the bottom layer, in which the red arrows and blue arrows indicate positive direction and negative direction of z component of the magnetization, respectively. When the spin-polarized current is perpendicularly injected into the nanodisk, the skyrmion pair starts to circularly move. Figure 2(b) shows the relationship between bottom skyrmion position and time with a spin-polarized current density of 1.0×10^{11} A/m^2, the fixed magnetic field is 300 mT, and the diameter of electrode is 30 nm. Figure 2(c) shows the guiding center of skyrmion pair at the same simulation parameters of current and magnetic field as those in Fig. 2(b), in which the red curve and the black curve represent the skyrmion position of top layer and that of the bottom layer, respectively. Moreover, the guiding center is described by the following equations:[38]

$$R_x = \frac{\iint xq\mathrm{d}x\mathrm{d}y}{\iint q\mathrm{d}x\mathrm{d}y}, \quad R_y = \frac{\iint yq\mathrm{d}x\mathrm{d}y}{\iint q\mathrm{d}x\mathrm{d}y}, \tag{3}$$

where q is the topological density. It is found that the trajectory radius of top skyrmion and bottom skyrmion are different, and the trajectory radius of top skyrmion is smaller than that of the bottom. This is due to the larger skyrmion size in the top layer with upward magnetic field. Therefore, the top skyrmion experiences a stronger repulsion from the nanodisk boundary, which makes it to move closer to the nanodisk center. Next, we obtain corresponding power spectrum by com-

puting fast Fourier transform of the oscillation of m_x, and figure 2(d) shows that the frequency is 1.07 GHz. According to the above results, we further investigate the factors influencing oscillation frequency under zero field in order to improve the performance of STNO based on SAF skyrmion pair. Firstly, figure 3(a) shows the relationship between the oscillation frequency and current density. When the diameter of electrode is fixed at 50 nm with a density of spin-polarized current of 4.5×10^{11} A/m^2, the oscillation frequency of bilayer skyrmion pair reaches up to 1.75 GHz. The skyrmion in the top layer will be annihilated as the current density is over the critical value. For each picked electrode diameter, the critical current density is different, which shows a decrease with the increase of the electrode diameter. The existance of critical current density finally leads to the maximum frequency for each electrode diameter. In our cases, the maximal frequencies of 1.53 GHz, 1.63 GHz, and 1.75 GHz for the electrode diameters of 20 nm, 30 nm, and 40 nm are obtained, respectively, which shows that the frequency increases with the electrode diameter increasing due to the stronger STT effect at the same current density. Next, we attempt to improve the strength of synthetic antiferromagnetic coupling between two free layers. It is found that the frequency can reach up to 5.2 GHz when the interlayer exchange coupling coefficient $\sigma = -1\times10^{-3}$ J/m^2 with a current density of 1.5×10^{12} A/m^2 as shown in Fig. 3(b). This is due to the more stable state of skyrimon pair at stronger couple, which enables the supporting of stronger effect of STT to avoid being annihilated. We also change angle θ to adjust the oscillation frequency, where the θ is defined as polarized angle of fixed layer as shown in Fig. 3(c). It is found that the oscillation frequency at $\theta = \pi/6$ is the highest in three picked angles, it can reach up to 2.01 GHz at a current density of 7.5×10^{11} A/m^2. For the STNO based on skyrmion pair in the nanodisk, the steady motion can be driven by current-induced force and expressed as[39]

$$\boldsymbol{F}_j \approx \pi^2 R_s \mu_0 B_j M_s t_z \boldsymbol{e}_z \times \boldsymbol{P}. \tag{4}$$

Here, $R_s \approx \Delta/\sqrt{2-2D/D_c}$ is the skyrmion radius, with $\Delta = \sqrt{A/K}$ being the domain wall width parameter and $D_c = 4\sqrt{AK}/\pi$; B_j relating to the applied current density j, described as $B_j = j\hbar p/2\mu_0 e M_s t_z$. However, the current-induced force F_j is proportional to $-\sin\theta$, where θ is the angle between the polarization vector and radial direction in the fixed layer. Hence, the current-induced force decreases with angle θ increasing, and the oscillation frequency decreases with the value of θ increasing. In this work, the angel θ is selected only as $\pi/6$, $\pi/4$, and $\pi/3$, so the oscillation frequency is highest at $\theta = \pi/6$.

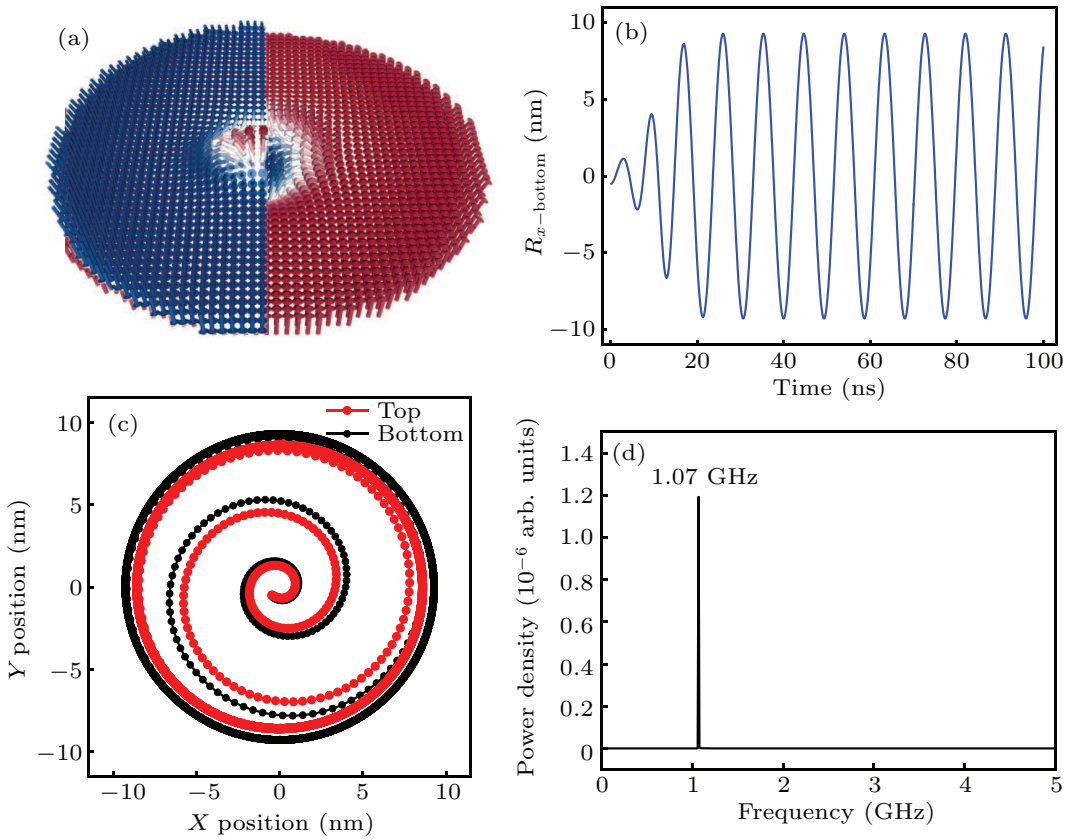


Fig. 2. (a) Initial state of synthetic antiferromagnetic skyrmion pair, where the core direction of top skyrmion and bottom skyrmion are upward and downward, respectively. (b) Time-dependent bottom layer skyrmion position. (c) Trajectory of skyrmion pair, where the red and black curves respectively represent top skyrmion and bottom skyrmion. (d) Power spectrum of x component of magnetization obtained by taking fast Fourier transform.

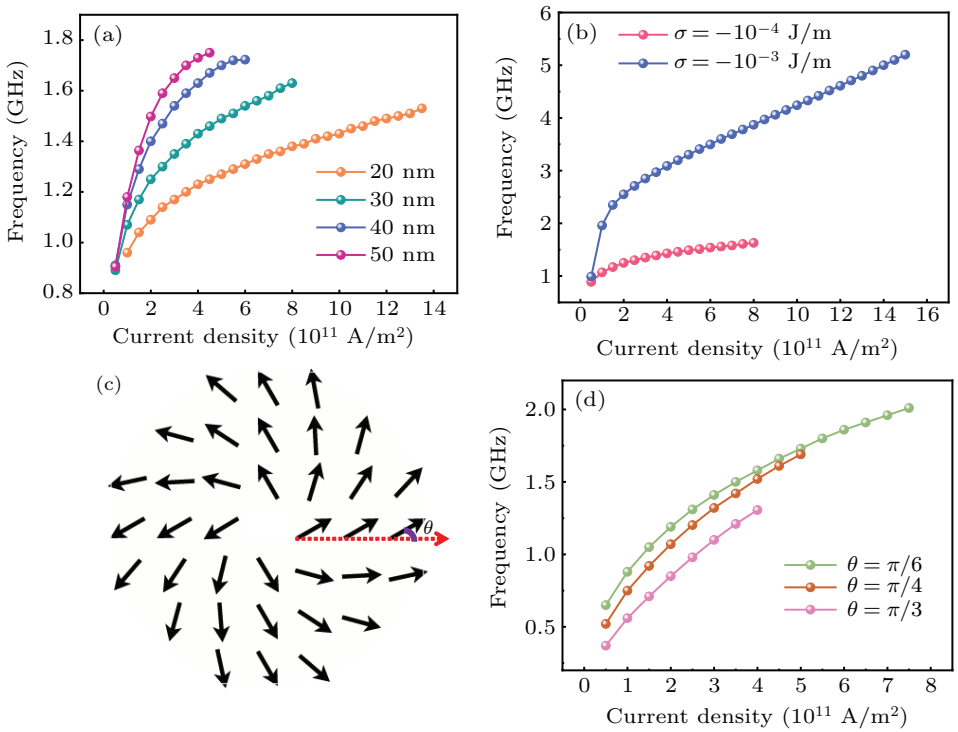


Fig. 3. (a) Plots of oscillation frequency *versus* current density for four different electrode diameters, with the interlayer exchange coupling coefficient fixed at -1×10^{-4} J/m^2. (b) Plots of oscillation frequency *versus* current density for two different interlayer exchange coupling strengths, with electrode diameter being 30 nm. (c) Magnetization configuration of fixed layer. (d) Curves of oscillation frequency *versus* current density for three different values of polarized angle θ, with interlayer exchange coupling coefficient and electrode diameter set to be -1×10^{-4} J/m^2 and 30 nm, respectively.

Next, we study the influence of skyrmion sizes on oscillation frequency. The results of Fig. 2 prove that the top-layer skyrmion enlarges and the bottom-layer skyrmion shrinks with the increase of upward fixed magnetic field. On the contrary, the downward field attempts to force the top skyrmion to shrink, while the skyrmion of the bottom layer to enlarge. For example, the diameter of top-layer skyrmion gradually increases as the positive fixed magnetic field rises, while the bottom-layer skyrmion keeps at 13 nm. This is mainly because the size of skyrmion is not only determined by the magnetic parameters, but also affected by the strength of the interlayer antiferromagnetic exchange coupling in this synthetic antiferromagnetic system. Therefore, the interlayer exchange coupling effective field can keep the bottom-layer skyrmion core in a small size without being annihilated, even under the action of the positive magnetic field. Figure 4(a) shows the relationship between the diameter of skyrmion and amplitude of magnetic field. When the absolute value of amplitude of the field is beyond 400 mT, the skyrmion pair cannot stably exist. The oscillation frequency varies with current density when the amplitude of upward magnetic field is set to be 200 mT, 300 mT, and 400 mT, respectively as shown in Fig. 4(b). On the one hand, the oscillation frequency increases as current density rises. On the other hand, the increasing of the magnetic field can also improve the frequency. It is worth noting that the oscillation frequency shows a sudden jump when the amplitude is set to be 400 mT, with the current density being 4.5×10^{11} A/m^2. In this case, the diameter of skyrmion in the top layer and the bottom layer are 25 nm and 15 nm, respectively.

In other word, the frequency will suddenly increase when the difference in diameter of skyrmion pair between two free layers is large enough. In order to prove this conclusion, we change the size of skyrmion by adjusting the value of DMI. The strong DM field also enlarges the size difference of bilayer skyrmion pair, so there also exists a sudden jump frequency when the value of DMI is 3.2 mJ/m^2 as shown in Fig. 4(c). The strong DM field also enlarges the size difference of bilayer skyrmion pair, so there also exists a sudden jump frequency when the value of DMI is 3.2 mJ/m^2 as shown in Fig. 4(c). This is mainly because the strong DMI effective field or fixed magnetic field increases the difference of skyrmion pair diameter, and the interlayer antiferromagnetic coupling strength will decrease between top-layer and bottom-layer skyrmions. When the difference of skyrmion pair size is big enough, in the top-layer skyrmion appears the breathing behavior under the higher current density. This breathing behavior excites the effect of an equivalent microwave field, thereby resulting in a peak shift of power spectrum. Thus, there is a sharp jump frequency that can be observed in Fig. 4(b) and also in Fig. 4(c), respectively, and this phenomenon will be further studied. Next, in order to further investigate the present conditions of multiple frequencies and single frequency, we pro-

vide the phase diagram of oscillation mode as a function of DMI and perpendicular magnetic field under different current densities. The blue circle represents single oscillation mode, and the STNO just outputs a single frequency microwave signal in these cases. In addition, the red up-side down triangle indicates that the skyrmion pair is annihilated at the edge of nanodisk. This is because the SAF skyrmion pair easily vanishes by strong effect of STT with poor stability. However, the green up triangle denotes mixed oscillation mode, *i.e.*, the STNO can output complex microwave signal with multiple oscillation frequency, which corresponds to these sudden jump frequencies in Figs. 4(b) and 4(c). The mixed mode exists only when the skyrmion size difference and current density are both large enough.

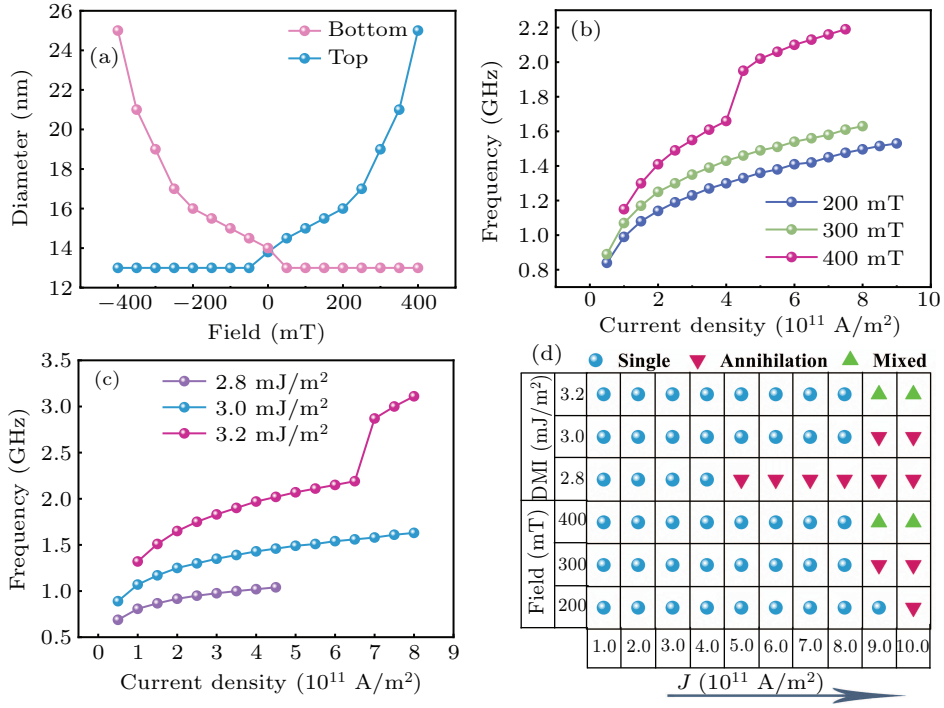


Fig. 4. (a) Variation of diameter with amplitude of magnetic field for top and bottom skyrmions. Curves of oscillation frequency *versus* current density for (b) three different upward magnetic fields (200 mT, 300 mT, and 400 mT) and (c) three different values of DMI (2.8 mJ/m^2, 3.0 mJ/m^2, and 3.2 mJ/m^2). (d) Phase diagram showing SAF skyrmion pair oscillation frequency mode under various current densities, amplitudes of fixed magnetic field, and values of DMI.

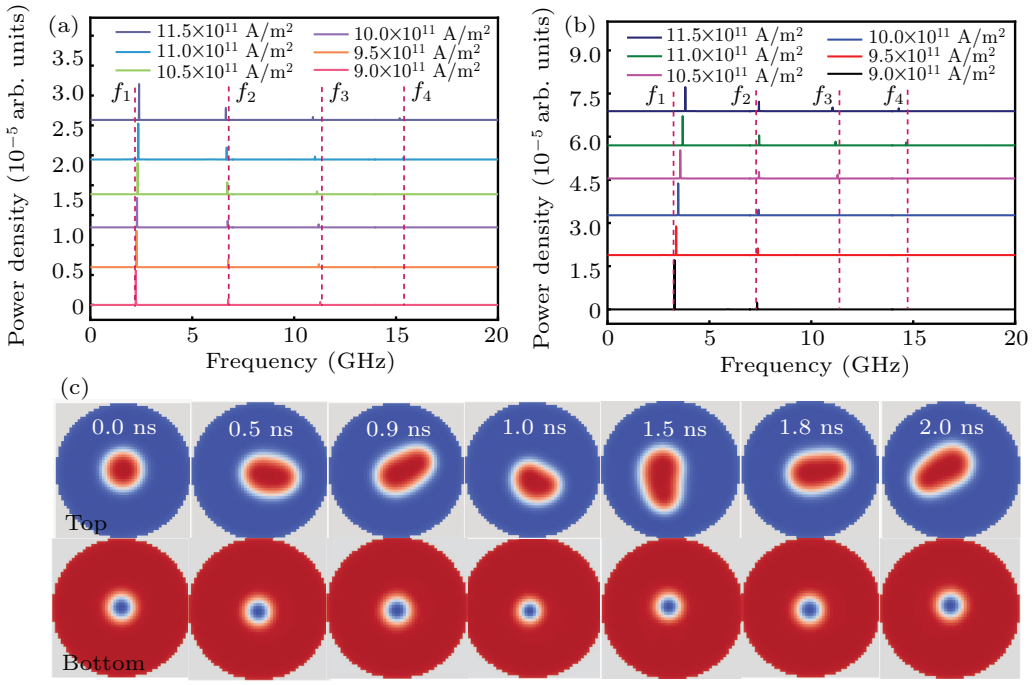


Fig. 5. Power spectrum of multiple frequency composite signal, with (a) magnetic field fixed at 400 mT and the value of DMI at 3.0 mJ/m^2, and (b) magnetic field fixed at 300 mT and the value of DMI at 3.2 mJ/m^2. (c) Rotation move process of SAF skyrmion pair while keeping breathing at different times, the first and second rows respectively refer to top layer and bottom layer.

In order to study the mixed mode with multiple oscillation frequencies, we provide the power spectrum. Figure 5(a) shows the multiple frequencies power spectrum when the magnetic field is set to be 400 mT, the value of DMI is fixed at 3.0 mJ/m^2. Figure 5(b) also displays the multiple frequencies power spectrum, while the amplitude of magnetic field set to be 300 mT, and the value of DMI fixed at 3.2 mJ/m^2. The current density varies from 9.0×10^{11} A/m^2 to 11.5×10^{11} A/m^2 both for Figs. 5(a) and 5(b). The oscillation frequency of strong peak f_1 increases as current density increases, which is caused by the precess of skyrmion pair under the effect of spin-polarized current. Moreover, the other frequencies of weak peak show small shift with respect to the main frequency. This is because the skyrmion of top layer presents the breath behavior as current density increases, which is similar to the effect of microwave magnetic field. Moreover, the amplitude of effective microwave magnetic field is enhanced with the increase of current density, which causes the new weak peaks to be excited.[40] Comparing Fig. 5(a) with Fig. 5(b), it is found that the peak shift in Fig. 5(b) is more obvious than in Fig. 5(a) in power spectrum. This is mainly because the DM effective field has more significant influence than magnetic field for skyrmion breathing behavior, which results in generating a larger amplitude of effective microwave magnetic field when the skyrmion shows an intenser breathing behavior. Thus, there appears a more shift of peak under the effect of stronger microwave magnetic field. The snapshot images of the dynamic process of skyrmion pair are shown in Fig. 5(c), where the top skyrmion displays an obvious breathing behavior during precession. Meanwhile, the bottom skyrmion also exhibits a tiny breathing, and stays a circular rotation near the center of the nanodisk.

4. Conclusions

In this work, we proposed a new kind of STNO based on SAF skyrmion pair. Firstly, our results showed that the output microwave signal can be adjusted by changing the area of electrode, interlayer exchange coupling strength, and the polarized angle of fixed layer. Then, we investigated the influence of the fixed magnetic field and DM effective field on the oscillation frequency of STNO. Interestingly, the larger difference of skyrmion pair size leads skyrmion pair to present the breathing behavior under larger current density, which excites other higher frequencies of weak peak. Hence, this kind of STNO can generate multiple frequency microwave signal. Our results open up possibilities for designing communication spintronic devices.

Data availability statement

The data supporting the findings of this study are available from the corresponding author upon reasonable request.

Acknowledgements

Project supported by the National Natural Science Foundation of China (Grant Nos. 12074158, 12174166, 12104197, and 12104124) and the Natural Science Foundation of Hebei Province, China (Grant No. A2021201008).

References

[1] Zeng Z M, Finocchio G and Jiang H W 2013 *Nanoscale* **5** 2219
[2] Fang B, Feng J F, Gan H D, Malmhall R, Huai Y M, Xiong R X, Wei H X, Han X F, Zhang B S and Zeng Z M 2016 *AIP Adv.* **6** 125305
[3] Rippard W H, Pufall M R, Kaka S, Russek S E and Silva T J 2004 *Phys. Rev. Lett.* **92** 027201
[4] Katine J A and Fullerton E E 2008 *J. Magn. Magn. Mater.* **320** 1217
[5] Dussaux A, Georges B, Grollier J, Cros V, Khvalkovskiy A V, Fukushima A, Konoto M, Kubota H, Yakushiji K, Yuasa S, Zvezdin K A, Ando K and Fert A 2010 *Nat. Commun.* **1** 8
[6] Grimaldi E, Dussaux A, Bortolotti P, Grollier J, Pillet G, Fukushima A, Kubota H, Yakushiji K, Yuasa S and Cros V 2014 *Phys. Rev. B* **89** 104404
[7] Ruotolo A, Cros V, Georges B, Dussaux A, Grollier J, Deranlot C, Guillemet R, Bouzehouane K, Fusil S and Fert A 2009 *Nat. Nanotechnol.* **4** 528
[8] Ma Y X, Song C K, Jin C D, Zhu Z T, Feng H M, Xia H Y, Wang J N, Zeng Z Z, Wang J B and Liu Q F 2020 *J. Phys. D: Appl. Phys.* **53** 195004
[9] Mohseni S M, Sani S R, Persson J, Nguyen T N A, Chung S, Pogoryelov Y, Muduli P K, Iacocca E, Eklund A, Dumas R K, Bonetti S, Deac A, Hoefer M A and Åkerman J 2013 *Science* **339** 1295
[10] Chung S, Mohseni S M, Sani S R, Iacocca E, Dumas R K, Nguyen T N A, Pogoryelov Y, Muduli P K, Eklund A, Hoefer M A and Åkerman J 2014 *J. Appl. Phys.* **115** 172612
[11] Zhang S F, Wang J B, Zheng Q, Zhu Q Y, Liu X Y, Chen S J, Jin C D, Liu Q F, Jia C L and Xue D S 2015 *New J. Phys.* **17** 023061
[12] Garcia-Sanchez F, Sampaio J, Reyren N, Cros V and Kim J V 2016 *New J. Phys.* **18** 075011
[13] Jin C D, Wang J B, Wang W W, Song C K, Wang J S, Xia H Y and Liu Q F 2018 *Phys. Rev. Appl.* **9** 044007
[14] Shen L C, Xia J, Zhao G P, Zhang X C, Ezawa M, Tretiakov O A, Liu X X and Zhou Y 2019 *Appl. Phys. Lett.* **114** 042402
[15] Zhou Y, Iacocca E, Awad A A, Dumas R K, Zhang F C, Braun H B and Åkerman J 2015 *Nat. Commun.* **6** 8193
[16] Feng Y H, Xia J, Qiu L, Cai X R, Shen L C, Morvan F J, Zhang X C, Zhou Y and Zhao G P 2019 *J. Magn. Magn. Mater.* **491** 165610
[17] Nagaosa N and Tokura Y 2013 *Nat. Nanotechnol.* **8** 899
[18] Mühlbauer S, Binz B, Jonietz F, Pfleiderer C, Rosch A, Neubauer A, Georgii R and Böni P 2009 *Science* **323** 915
[19] Yu X Z, Onose Y, Kanazawa N, Park J H, Han J H, Matsui Y, Nagaosa N and Tokura Y 2010 *Nature* **465** 901
[20] Huang S X and Chien C L 2012 *Phys. Rev. Lett.* **108** 267201
[21] Heinze S, von Bergmann K, Menzel M, Brede J, Kubetzka A, Wiesendanger R, Bihlmayer G and Blügel S 2011 *Nat. Phys.* **7** 713
[22] Jiang W J, Upadhyaya P, Zhang W, Yu G Q, Jungfleisch M B, Fradin F Y, Pearson J E, Tserkovnyak Y, Wang K L, Heinonen O, Velthuis S G E T and Hoffmann A 2015 *Science* **349** 283
[23] Boulle O, Vogel J, Yang H X, Pizzini S, Chaves D D S, Locatelli A, Menteş T O, Sala A, Buda-Prejbeanu L D, Klein O, Belmeguenai M, Roussigné Y, Stashkevich A, Chérif S M, Aballe L, Foerster M, Chshiev M, Auffret S, Miron I M and Gaudin G 2016 *Nat. Nanotechnol.* **11** 449
[24] Zhang X C, Zhou Y and Ezawa M 2016 *Nat. Commun.* **7** 10293
[25] Liu X H, Edmonds K W, Zhou Z P and Wang K L 2020 *Phys. Rev. Appl.* **13** 014059

[26] Liu X H, Deng Y C, Lan X K, Li R Z and Wang K Y 2021 *Sci. China-Phys. Mech. Astron.* **64** 267511
[27] Dohi T, DuttaGupta S, Fukami S and Ohno H 2019 *Nat. Commun.* **10** 5153
[28] Qiu L, Shen L C, Zhang X C, Zhou Y, Zhao G P, Xia W X, Luo H B and Liu J P 2021 *Appl. Phys. Lett.* **118** 082403
[29] Feng Y H, Zhu H K, Zhang X and Xiang G 2022 *J. Magn. Magn. Mater.* **543** 168641
[30] Fert A, Reyren N and Cros V 2017 *Nat. Rev. Mater.* **2** 17031
[31] Nagaosa N and Tokura Y 2013 *Nat. Nanotech.* **8** 899
[32] Sampaio J, Cros V, Rohart S, Thiaville A and Fert A 2013 *Nat. Nanotech.* **8** 839
[33] Dohi T, DuttaGupta S, Fukami S and Ohno H 2019 *Nat. Commun.* **10** 5153
[34] Donahue M J and Porter D G 1999 *OOMMF User's Guide* (Gaithersburg, MD: US Department of Commerce, Technology Administration, National Institute of Standards and Technology)
[35] Brataas A, Kent A D and Ohno H 2012 *Nat. Mater.* **11** 372
[36] Jin C D, Zhang C L, Song C K, Wang J S, Xia H Y, Ma Y X, Wang J N, Wei Y R, Wang J B and Liu Q F 2019 *Appl. Phys. Lett.* **114** 192401
[37] Zhang X C, Zhou Y and Ezawa M 2016 *Nat. Commun.* **7** 10293
[38] Papanicolaou N and Tomaras T N 1991 *Nucl. Phys. B* **360** 425
[39] Shen L C, Xia J, Zhao G P, Zhang X C, Ezawa M, Tretiakov O A, Liu X X and Zhou Y 2019 *Appl. Phys. Lett.* **114** 042402
[40] Song C K, Ma Y X, Jin C D, Xia H Y, Wang J N, Zeng Z Z, Wang J B and Liu Q F 2020 *Phys. Status Solidi RRL* **14** 2000249